catalysts

MDPI

Article

Enhanced Photocatalytic Activity of Hierarchical Bi_2WO_6 Microballs by Modification with Noble Metals

Zhenhao Li [1,2], Kunlei Wang [3,4], Jinyue Zhang [1,2], Ying Chang [1,2], Ewa Kowalska [3,*] and Zhishun Wei [1,2,*]

1 Hubei Provincial Key Laboratory of Green Materials for Light Industry, New Materials and Green Manufacturing Talent Introduction and Innovation Demonstration Base, Hubei University of Technology, Wuhan 430068, China; hobbyli1997@163.com (Z.L.); jeson020109@icloud.com (J.Z.); cy0025@hbut.edu.cn (Y.C.)
2 School of Materials and Chemical Engineering, Hubei University of Technology, Wuhan 430068, China
3 Institute for Catalysis, Hokkaido University, Sapporo 001-0021, Japan; kunlei@cat.hokudai.ac.jp
4 Northwest Research Institute, Co., Ltd. of C.R.E.C., Lanzhou 730000, China
* Correspondence: kowalska@cat.hokudai.ac.jp (E.K.); wei.zhishun@hbut.edu.cn (Z.W.)

Abstract: Visible-responsive photocatalysts for environmental purification and fuel generation are, currently, highly sought after. Among the possible candidates, Bi_2WO_6 (BWO) has been considered due to its efficient light harvesting, stability, and promising activities. Here, hierarchical BWO microballs have been prepared using a hydrothermal method, and additionally modified with deposits of noble metals (gold, silver, copper, palladium and platinum) by the photodeposition method. The structure, morphology, photoabsorption properties, and surface composition of bare and metal-modified BWO samples were investigated by XRD, SEM, DRS and XPS analyses. The photocatalytic activity was evaluated by the oxidative degradation of model dye (methyl orange (MO)) under UV/vis, and hydrogen generation under vis and/or UV irradiation. It was found that hierarchical morphology is detrimental for high photocatalytic activity in both tested systems, resulting in the improved degradation of MO (ca. 65% during 90 min of UV/vis irradiation), and hydrogen evolution (0.1 and 0.4 μmol h^{-1} under vis and UV/vis irradiation, respectively). Moreover, the type of noble metal and its properties influence the overall photocatalytic performance. It was found that, under UV/vis irradiation, only platinum accelerates hydrogen evolution, whereas under vis irradiation the activity follows the order: BWO < BWO/Cu < BWO/Ag < BWO/Pt < BWO/Pd < BWO/Au. It was concluded that zero-valent metal is recommended for high vis response, probably due to plasmonic photocatalysis, efficient light harvesting ability, and co-catalytic role.

Keywords: Bi_2WO_6; hierarchical microballs; flake balls; noble metals; plasmonic photocatalysis; vis response; hydrogen generation; dye degradation

check for updates

Citation: Li, Z.; Wang, K.; Zhang, J.; Chang, Y.; Kowalska, E.; Wei, Z. Enhanced Photocatalytic Activity of Hierarchical Bi_2WO_6 Microballs by Modification with Noble Metals. *Catalysts* **2022**, *12*, 130. https://doi.org/10.3390/catal12020130

Academic Editor: Sylwia Mozia

Received: 9 December 2021
Accepted: 17 January 2022
Published: 21 January 2022

1. Introduction

Global energy and environmental crises are considered the most urgent problems to be solved. Among various solutions, hydrogen has been proposed as an alternative fuel due to its high specific energy (three times the heating value of petroleum) and environmentally friendly nature, i.e., its combustion results in the formation of only a clean product—water ("maker of water" in Greek) [1]. However, the most significant is the clean production of hydrogen itself, and thus, usage of fossil fuels should be avoided. Accordingly, green processes, such as photocatalysis, have been considered for hydrogen generation [2–5]. For example, semiconductor photocatalysis might solve both energy and environmental problems (including ones related to drinking water), particularly when performed under natural solar radiation [6–8]. The photocatalysts could split water into hydrogen and oxygen, as well as decompose all pollutants (microorganisms and organic and inorganic compounds), and thus heterogeneous photocatalysis has attracted a lot of attention in recent decades [9–12]. Among the various semiconductors, titanium(IV) oxide (TiO_2, titania, titanium dioxide) has been the most explored due to its low cost,

high activity, low toxicity, abundance, and pollution-free nature [13–15]. However, titania also has some shortcomings. First, titania is only responsive to the UV part of the solar spectrum due to its large bandgap, and thus, only a minor part of solar energy can be efficiently used (3–4%). Second, the recombination of charge carriers results in a lower than 100% quantum efficiency of photocatalytic reactions. Third, the most active titania photocatalysts are usually in the form of fine particles, which raises some problems with photocatalyst reuse and circulation (high costs of ultrafiltration). In contrast, the application of immobilized photocatalysts is connected with a low specific surface area, and thus a decrease in photocatalytic efficiency [16–18]. Therefore, the synthesis of highly efficient materials for the broad range of solar radiation, and easy recyclability, is a hot topic of present studies. For example, wide-bandgap semiconductors were either surface modified [19–21] or doped [22–24] with various elements, as well as coupled with other semiconductors of narrower bandgaps [25–28]. Moreover, new chemical compounds have been synthesized and proposed as efficient photocatalysts, such as oxynitrides [29], graphitic carbon nitride [30], germanium nitride [31], and graphene derivatives [32]. However, a narrower bandgap allows for fast charge carriers' recombination. Therefore, these new materials have also been further modified/coupled (e.g., MoS_2-C-g-C_3N_4 [33]) to obtain an efficient transfer of charge carriers (via type II heterojunction or/and Z-scheme [5,34]), and thus, high yields of photocatalytic reactions.

For example, as a material with a narrower bandgap than that of titania, bismuth-based compounds have attracted much attention [35]. It has been shown that bismuth tungstate (Bi_2WO_6, BWO) with a layered structure of WO_6 and $[Bi_2O_2]^{2+}$ (perovskite-like plates) has exhibited good photocatalytic efficiency under vis irradiation [36–39]. However, the photogenerated charge carriers recombine easily, and thus result in a low photocatalytic efficiency. Accordingly, many methods have been used for BWO modification, such as morphology optimization [37,38,40,41], elemental doping [42,43], surface modification (e.g., with noble metals [44–47]), and the formation of heterojunctions, e.g., Bi_2WO_6/Zn-Al [48], $Bi_2Fe_4O_9/Bi_2WO_6$ [49], MoS_2/Bi_2WO_6 [50].

It is known that noble metals can effectively improve the photocatalytic performance of photocatalysts, being an electron pool, and thus hinder the recombination of charge carriers. Various semiconductors with deposited noble metals have already been prepared, such as titania [51–54] and other photocatalysts, e.g., Bi_2MoO_6 nanoplates (Ag) [55], BiOCl nanospheres (Ag) [56], carbon nitride nanorods (Au) [57], g-C_3N_4 (Cu) [58], and BiOBr (Pd) [59]. It should be mentioned that though modification with noble metals (to improve UV-photocatalytic activity) has been known for more than 40 years, novel research has been started recently on plasmonic photocatalysis, in which noble metals play another function, i.e., the activation of wide-bandgap semiconductors towards a vis response due to plasmonic properties [60–62].

Although both pristine and modified BWO samples have been investigated for various photocatalysts reactions, there are no reports showing a direct comparison between BWO photocatalysts modified with different noble metals. In this study, the influence of five metals (Au, Ag, Cu, Pd and Pt) on the properties, and thus overall activity, of BWO (in the form of hierarchical microballs for cheap recycling) is investigated for the first time. The photocatalytic activity has been tested for hydrogen generation and the decomposition of methyl orange (MO; common and toxic dye [63]) since both "green" fuel production and environmental purification (especially the degradation of organic compounds) are the most urgent problems facing humanity.

2. Results and Discussion

2.1. Characterization of Samples

The successful preparation of BWO by a hydrothermal method has been confirmed by XRD analysis, as shown in Figure 1. All pristine samples, prepared at different temperatures, show almost identical diffraction patterns with clear peaks at ca. 28.3, 32.8, 47.2, 55.8, 58.5, 68.7, 76.1 and 78.5 degrees, indicating (131), (002), (202), (133), (262), (004), (333) and (460)

crystal planes of russellite Bi_2WO_6, respectively. An increase in hydrothermal temperature results in peak sharpening, suggesting that larger crystallites have been formed. Indeed, Scherrer analysis confirms that the crystallites prepared at 140 °C reach 13.6 nm, whereas higher temperatures (180 °C and 160 °C) cause the formation of larger crystallites (14.8 nm and 16.2 nm, respectively).

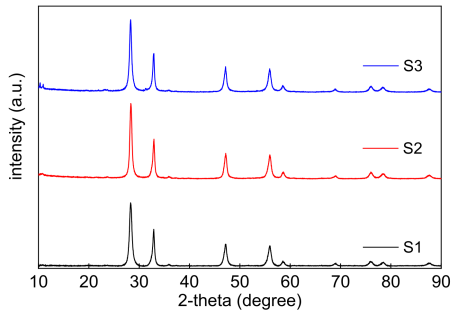

Figure 1. XRD patterns of BWO samples prepared at different temperatures.

The microscopic observations revealed that a hydrothermal reaction results in the formation of microballs composed of nanosheet subunits, as shown in Figure 2. The best morphology was obtained at the lowest temperature of reaction (140 °C), as the S1 sample exhibits a regular spherical flower-like structure with a relatively uniform size distribution, and the microballs are composed of flat sheets (Figure 2a,b). A worsening of the morphology was noticed after increasing the temperature of the hydrothermal reaction. Accordingly, though microballs in the S2 sample are still mainly spherical (Figure 2c,d), the substructured sheets are irregular and uneven in size. Finally, the worst morphology was achieved for the S3 sample (Figure 2e,f), for which the spherical morphology is no longer obvious, and the structure of built-in flakes is likewise incomplete. Based on the presented data, it has been found that the spherical structure of BWO was destroyed gradually, and substructure sheets were fragmented by increasing the hydrothermal reaction temperature, indicating that temperature is crucial for the morphology of BWO samples. Accordingly, the S1 sample with the best morphology (and highest photocatalytic efficiency, as discussed further) was selected for the modification with noble metals.

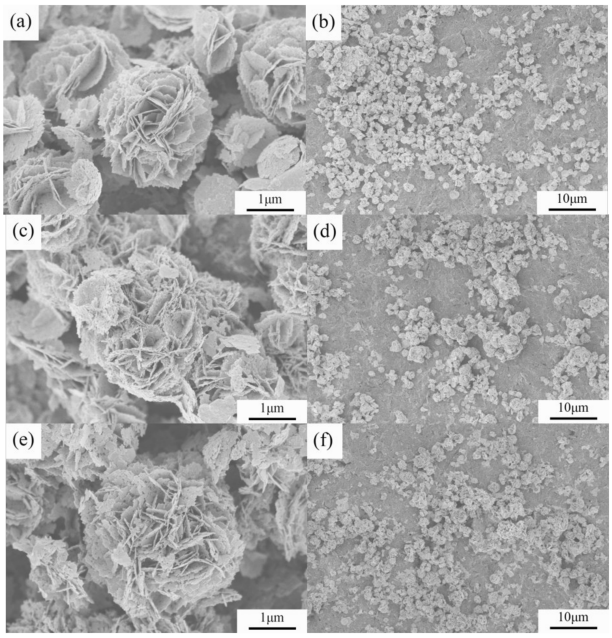

Figure 2. BWO samples obtained at different temperatures: (**a**,**b**) S1 (140 °C), (**c**,**d**) S2 (160 °C) and (**e**,**f**) S3 (180 °C).

The XPS was used for the surface characterization of both pristine and modified samples. All samples are composed of Bi_2WO_6 (Figure 3). Although slight shifts in the binding energy were observed with an increase in the temperature of the hydrothermal reaction, it seems to be irrelevant for the chemical composition, as previously reported [64]. Taking the S1 sample as an example, the XPS spectra of Bi 4f and W 4f show the binding energies of 159.0 eV (Bi $4f_{7/2}$), 164.31 eV (Bi $4f_{5/2}$), 37.33 eV (W $4f_{5/2}$) and 35.2 eV (W $4f_{7/2}$), indicating that bismuth and tungsten exist in tri- [65] and six-valent [66] oxidation states, respectively. In the case of the oxygen (O 1s) spectrum, two peaks at 530.05 eV and 531.53 eV could be seen, relating to W-O and Bi-O, respectively. Thus, the chemical formula of Bi_2WO_6 was confirmed [67].

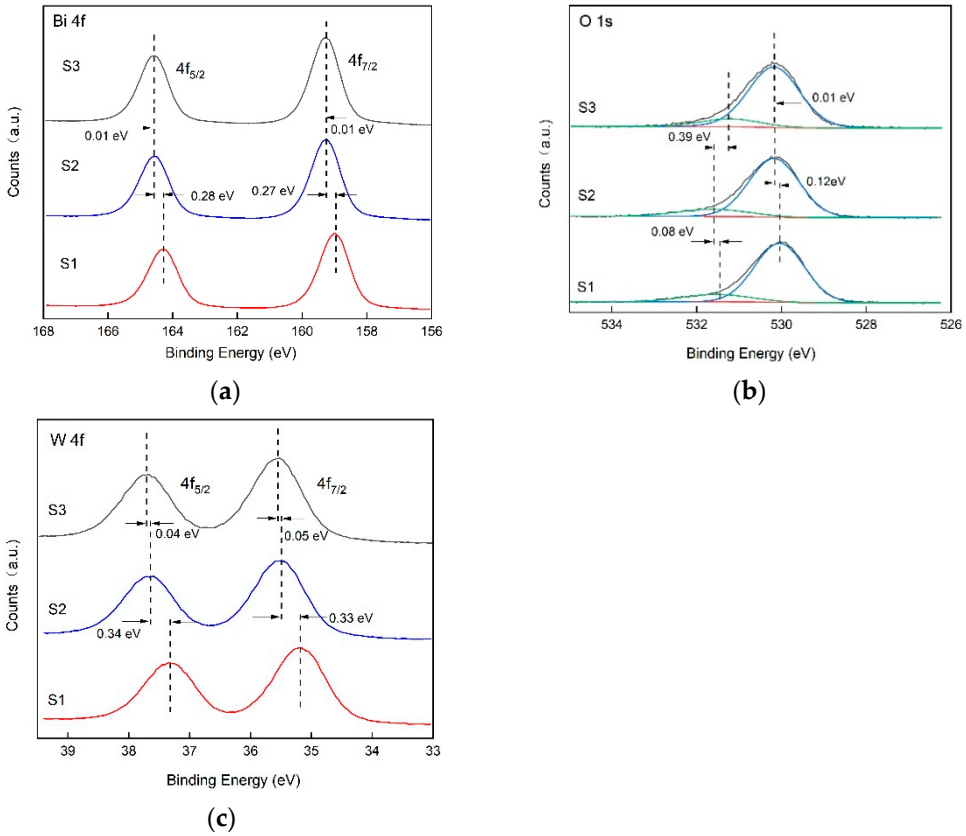

Figure 3. XPS results for: (**a**) Bi 4f, (**b**) O 1s and (**c**) W 4f.

In the case of modified S1 samples, XPS data have confirmed that noble metals were efficiently loaded onto the BWO surface, as shown in Figure 4 and Table 1. It has been found that silver exists in two oxidation forms, i.e., Ag^+ and Ag(0), with binding energies of 367.51 eV and 368.3 eV, respectively, with the oxidized form being predominant (ca. 90%). In contrast, three forms of gold, i.e., Au(δ+), Au(0) and Au(δ−), were observed with binding energies of 82.89 eV, 83.6 eV and 83.94 eV, respectively. Here, the zero-valent form of gold is the most predominant, reaching 92%. In the case of copper, only its oxidized forms could be detected, i.e., Cu^+ (932.16 eV [68]; 58%) and Cu^{2+} (932.28 eV [68]; 42%), confirming the instability of zero-valent copper under ambient conditions [69–71]. As expected, palladium and platinum exist mainly in the zero-valent form, reaching 80% and 79%, respectively, making up the minority of the oxidized forms of metals (probably PdO [72] and Pt(δ+) [68]). Similar data have been commonly found for semiconductors modified with noble metals, where less noble metals (silver and copper) exist, predominantly in the oxidized forms, whereas precious metals (gold, platinum and palladium) are present as zero-valent deposits [69–71,73–75]. It must be underlined that, during photodeposition (anaerobic environment), though metal cations are reduced efficiently, forming zero-valent NPs (as confirmed by the color change, e.g., violet for Cu/S1 due to the plasmonic properties), the

direct contact of the sample with air (after photodeposition) results in the partial oxidation (surface) of less noble metals.

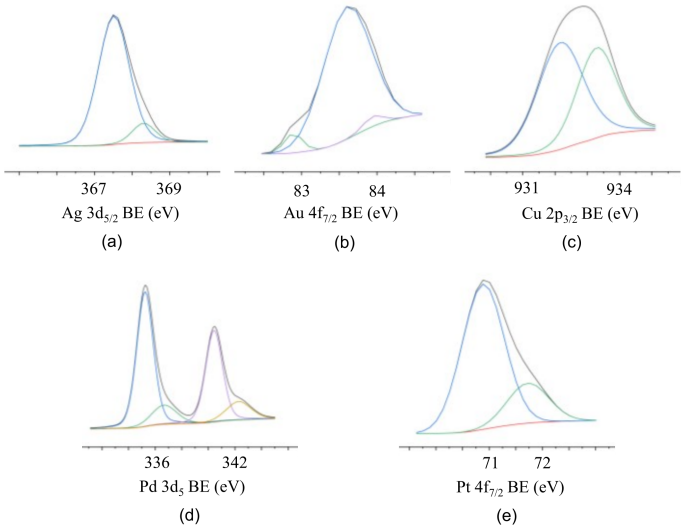

Figure 4. XPS results for S1 sample modified with noble metals: (**a**) Ag $3d_{5/2}$, (**b**) Au $4f_{7/2}$, (**c**) Cu $2p_{3/2}$, (**d**) Pd $3d_5$ and (**e**) Pt $4f_{7/2}$.

Table 1. Surface composition of pristine and modified S1 samples.

Samples		S1	Pt/S1	Au/S1	Ag/S1	Cu/S1	Pd/S1
content (at%)	Bi	17.3	20.5	20.3	18.2	18.2	18.9
	C	31.6	26.8	21.1	28.0	25.3	23.1
	O	43.8	43.6	51.1	46.2	49.1	49.8
	W	7.3	8.7	7.4	7.1	7.0	7.4
	Pt	-	0.4	-	-	-	-
	Au	-	-	0.1	-	-	-
	Ag	-	-	-	0.5	-	-
	Cu	-	-	-	-	0.4	-
	Pd	-	-	-	-	-	0.8

The photoabsorption properties of bare and modified BWO materials are presented in Figure 5. It has been confirmed that BWO can absorb visible light up to ca. 450 nm, which corresponds to bandgap of ca. 2.75 eV (evidently narrower than that in titania). Moreover, as expected (considering the same crystalline form and similar crystallite sizes), all bare samples (S1–S3) show almost identical photoabsorption properties (Figure 5a). Furthermore, a significant increase in vis absorption was observed after BWO modification with noble metals. The characteristic plasmonic peaks (localized surface plasmon resonance; LSPR) were observed for Au/S1 and Ag/S1 at ca. 545 nm and ca. 490 nm, respectively, suggesting the formation of fine gold NPs (10–20 nm) and larger silver deposits (ca. 80 nm [76]). It should be mentioned that the LSPR wavelength is influenced by both the properties (size/shape/surroundings) and the type of the metal, and thus smaller and spherical NPs possess LSPR at shorter wavelengths [77]. For example, spherical NPs of 10–20 nm show LSPR at ca. 200 nm [78], 395–405 nm [79], 420–430 nm [80], 530–540 nm [81] and 560–570 nm [82] when composed of palladium, platinum, silver, gold, and copper, respectively. The formation of a Ag_2O/Bi_2WO_6 heterojunction should also be considered as a similar photoabsorption feature has been observed (the peak at ca. 500 nm) for other semiconductors (e.g., titania) modified with silver(I) oxide (even though a very different photoabsorption feature of sole Ag_2O is obtained due to its dark brown color) [26]. In the case of samples containing palladium and platinum, it is difficult to observe a clear LSPR peak (expected at UV range), and thus the efficient light absorption in the whole vis region

could be caused by either the presence of large particles or scattering of the light on the metal deposits. In contrast, though a clear peak at near IR was observed for Cu/S1 sample, its origin is due to CuO rather than zero-valent copper (the lowest light absorption at main LSPR wavelength of 560 nm for spherical Cu NPs), thus it has been confirmed (similar to XPS data) that copper exists mainly in the oxidized form [83–86].

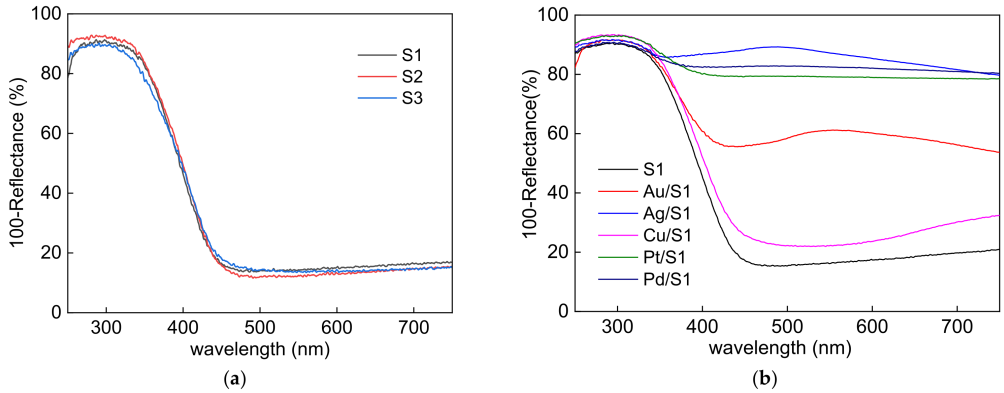

Figure 5. DRS spectra of: (**a**) bare BWO samples and (**b**) bare and modified S1 samples.

2.2. Photocatalytic Activity

The photocatalytic activities of obtained photocatalysts were evaluated in two reaction systems: (1) the decomposition of MO (aerobic environment) and (2) generation of hydrogen (anaerobic environment) under vis and/or UV irradiation.

First, the photocatalytic activity of bare BWO samples was examined in comparison to two reference samples, pure commercial WO_3 (purchased by Aladdin (Vienna, VA, USA)) and Bi_2WO_6 (homemade), and the obtained data for MO degradation are presented in Figure 6. It is obvious that both reference samples are barely active, which is reasonable considering that oxides with narrower bandgap than that in titania suffer from charge carriers' recombination due to negligible activity for the one-electron reduction of oxygen. Conduction band (CB) position must be more negative than −0.284/−0.046 V vs. NHE ($O_2 + e^- = O_2^-$ (aq.)/$O_2 + H^+ + e^- = HO_2$ (aq.)) for the consumption of photogenerated electrons and degradation of organic matter by photogenerated holes [87,88]. In contrast, hierarchical microballs exhibit superior photocatalytic activity, which correlates with their morphology; i.e., the most active sample (S1) has the best morphology. It should be emphasized that all samples possess nearly identical properties, such as the crystallite size, crystallinity, composition and photoabsorption properties, except for morphology, and thus the difference in the activity should be caused by the morphology. Accordingly, it could be concluded that "flake balls" are responsible for the oxidative decomposition of organic compounds with the possibility of a multi-electron transfer mode, as suggested by Hori et al. [89].

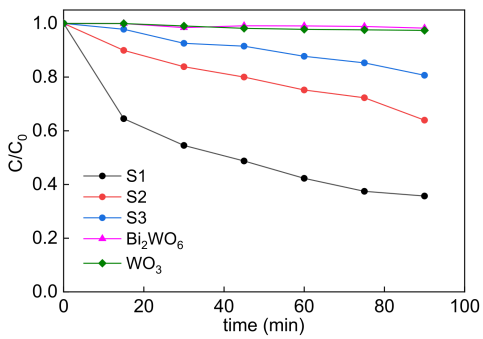

Figure 6. Photocatalytic activity of MO discoloration under UV/vis irradiation for synthesized (S1, S2, S3) and reference (commercial WO_3 and homemade BWO) samples.

Similarly, S1 sample shows to be the most active for hydrogen evolution, as shown in Figure 7a. However, the reaction rates for S1 and S2 photocatalysts are very similar, reaching 0.38 μmol/h and 0.33 μmol/h, respectively. In contrast, a twice-as-slow rate has been obtained for S3 sample with partly destroyed sheets' structure. Therefore, it is obvious that the morphology is detrimental to achieving a high photocatalytic activity. However, it seems that a perfect sheet structure is more important for hydrogen generation, whereas microball morphology is detrimental for the decomposition of organic compounds.

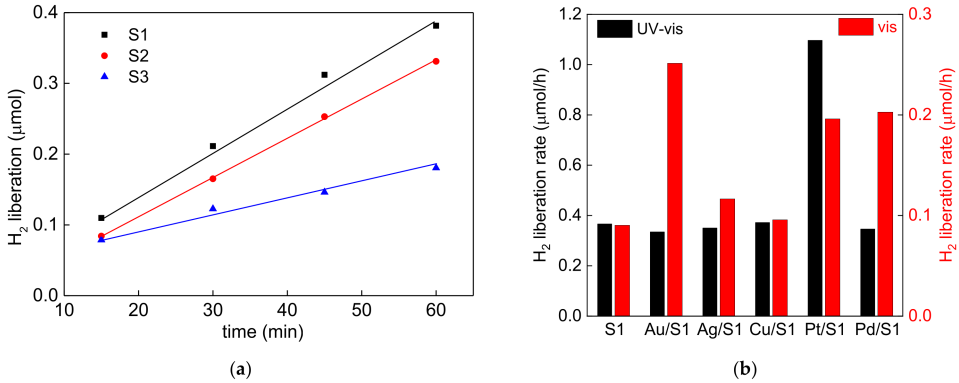

Figure 7. Photocatalytic hydrogen generation on: (**a**) BWO microballs (S1, S2 and S3) under UV/vis irradiation, and (**b**) bare and modified S1 samples under UV/vis (black) and vis (red) irradiation.

Since the photocatalytic activity data for pristine samples have indicated that S1 is the most active, this sample was selected for the modification with noble metals, and the obtained results are presented in Figure 7b. Interestingly, only modification with platinum resulted in a significant generation of hydrogen under UV/vis irradiation. It must be emphasized that this differs greatly from the titania case, for which modification with any noble metal increases the photocatalytic activity for hydrogen evolution [70,81,90–94]. It has been proposed that molecular hydrogen is directly formed on the deposits of noble metals [95,96]. It should be mentioned that the low activity of BWO for hydrogen evolution has already been suggested (even after modification with platinum) [97], likely resulting from insufficient redox properties (too positive a conduction band). However, there are also some reports showing the photocatalytic activity of BWO for hydrogen generation [98]. Here, hierarchical microballs modified with platinum have exhibited a noticeable generation of hydrogen. Accordingly, it is proposed that platinum might work as an electron pool and a catalyst (dark) for the formation of molecular hydrogen.

Interestingly, the activity under sole vis irradiation is quite different, where gold-modified sample shows the highest activity. Additionally, samples with platinum and palladium are much more active than pristine BWO sample. Therefore, it might be concluded that zero-valent metals are responsible for efficient hydrogen evolution. Two reasons could be considered, i.e., (i) plasmonic photocatalysis or (ii) catalytic "dark" reaction on the metallic deposits. Considering the catalytic "dark" properties of metals (volcano plot), the activity should be in the following order: platinum > palladium > gold $\geq$ copper > silver [99]. Here, Au/S1 is the most active, with a broad plasmonic peak (500–650 nm), and thus it is expected that the efficient light absorption by plasmonic metal might be the main reason for enhanced activity under vis irradiation. There are two mechanisms of plasmonic photocatalysis, i.e., an energy transfer, and an electron transfer [60,100–102]. It seems that both could be involved as even a slight overlapping of photoabsorption bands (LSPR and semiconductor) could result in the energy transfer. Moreover, the double function of noble metals must also be considered: (i) plasmonic sensitizer, and (ii) catalytic center for hydrogen generation. Obviously, zero-valent metals are crucial for both activities. The slight increase in activity by silver modification might also result from the presence of zero-valent silver (ca. 10%). Of course, the formation of heterojunctions between two oxides, e.g., Ag_2O/BWO, Cu_2O/BWO and CuO/BWO, could also be inspected. However,

the inactivity of the copper-modified sample suggests that these types of heterojunctions are not working for hydrogen evolution (again, in contrast to the case of titania [26,27,103,104]). Therefore, it could be concluded that zero-valent noble metals are necessary for the efficient enhancement of photocatalytic efficiency of BWO under vis light.

3. Materials and Methods

3.1. Preparation of BWO

$Na_2WO_4 \cdot 2H_2O$, $Bi(NO_3)_3 \cdot 5H_2O$, and cetyltrimethylammonium bromide (CTAB) were purchased from Aladdin Bio-Chem Technology Co., Ltd. (Shanghai, China) (AR, 99%), and used without further treatment. BWO was synthesized by hydrothermal reaction. In brief, 2 mmol of $Na_2WO_4 \cdot 2H_2O$ and 4 mmol of $Bi(NO_3)_3 \cdot 5H_2O$ were placed in a 100 mL beaker, to which 60 mL deionized water was added, and then the content was stirred magnetically for half an hour. Afterwards, 0.05 g of CTAB was added, the content was stirred for 15 min, and the white suspension (the pH value of 1.44) was poured to a 100 mL Teflon tube. The tube was placed inside the oven for a 24 h hydrothermal reaction, performed at three different temperatures. The final product was collected, washed with deionized water, centrifuged, and freeze dried. The obtained yellowish powders were marked as S1, S2 and S3 for BWO samples prepared at 140 °C, 160 °C and 180 °C, respectively.

3.2. Modification of BWO with Noble Metals

$H_2PtCl_6 \cdot 6H_2O$, $HAuCl_4 \cdot 3H_2O$, $AgNO_3$, $CuSO_4 \cdot 5H_2O$, and K_2PdCl_6 were purchased from Aladdin company (Vienna, VA, USA) (AR, 99%). For the modification, S1 sample (prepared at 140 °C) and aqueous solution (40 g/L) of respective salts, i.e., $H_2PtCl_6 \cdot 6H_2O$ (Aladdin ((Vienna, VA, USA)), $HAuCl_4 \cdot 3H_2O$ (Aladdin (Vienna, VA, USA)), $AgNO_3$ (Aladdin (Vienna, VA, USA)), $CuSO_4 \cdot 5H_2O$ (Aladdin (Vienna, VA, USA)) and K_2PdCl_6 (Aladdin (Vienna, VA, USA)), were used, and the obtained samples were named accordingly, i.e., Pt/S1, Au/S1, Ag/S1, Cu/S1 and Pd/S1. In brief, 500 mg of S1 sample was added to a glass tube containing 25 mL of water/methanol (1:1) solution, and then the aqueous solution of noble metal (2 wt% of noble metal in respect to BWO) was added gradually by a micropipette under continuous stirring. Afterwards, the glass tube was covered with a latex stopper, and argon gas was purged through a thin plastic tube placed at the bottom of the tube for 15 min to remove oxygen (working as an electron scavenger). Then, the tube was sealed and wrapped with tape. The tube was irradiated with a xenon lamp (300 W, 100 mW cm^{-2}, 10 cm distance from the lamp) and the content was continuously stirred during 1 h irradiation. Finally, the obtained powder was collected after finishing operations, i.e., centrifugation, washing (2 times with ethanol and 2 times with deionized water), freeze drying and grinding.

3.3. Sample Characterization

The crystalline properties of samples were examined by X-ray diffraction (XRD; PANalytical Empyrean X-ray diffractometer). The morphology was observed with scanning electron microscopy (SEM, SU8010, Hitachi Limited Company, Tokyo, Japan) The surface properties (chemical composition and state of elements) were evaluated by X-ray photoelectron spectroscopy (XPS, PHI5000, ULVAC-PHI, Inc, Kanagawa, Japan) with C 1s (284.8 eV) as a reference for binding energy. The photoabsorption features were estimated by UV/vis diffuse reflectance spectroscopy (DRS, UV3600, Shimadzu Corporation, Kyoto, Japan).

3.4. Photocatalytic Activity

The photocatalytic performance was evaluated for two model reactions: oxidation (photodegradation of methyl orange) and reduction (generation of hydrogen). For the oxidative decomposition of methyl orange, a 300 W xenon lamp (100 mW cm^{-2}) was settled in 15 cm distance from the glass reactor. First, 150 mg of photocatalyst and 150 mL of MO (20 mg/L) were placed into the glass reactor, stirred for half an hour in a dark box to reach the equilibrium of adsorption/desorption, and then irradiated. Every 15 min the portion of

suspension (ca. 6 mL) was withdrawn from the reactor, centrifuged for 5 min (5000 rpm), and then the absorbance of the supernatant was analyzed by a UV/vis spectrophotometer (UV-1800PC).

For hydrogen generation, a closed glass reaction system—an automatic on-line trace gas analysis system (Labsolar-6A, Beijing Perfectlight Technology Co., Ltd., Beijing, China) was used. First, the photocatalyst (50 mg) was added to 100 mL aqueous solution with triethanolamine (TEOA, 10 vol%, a sacrificial electron donor). The reactor was evacuated with a vacuum pump and irradiated with a xenon lamp (300 W, 100 mW cm^{-2}). For vis activity measurements, a cut-off filter ($\lambda > 420$ nm) was installed on the front of the lamp. The amount of generated hydrogen was determined by on-line gas chromatography system (GC7900II).

4. Conclusions

BWO hierarchical microballs can be easily prepared by a simple hydrothermal method and then modified with nanoparticles of different noble metals. It has been found that a uniform morphology of microballs, composed of similar sheets, is necessary for the efficient degradation of methyl orange under UV/vis, which results in 65% decomposition over 90 min of illumination. In contrast, the flat sheet surface seems detrimental to hydrogen generation, as two different samples (S1 and S2) have caused similar effects, generating ca. 0.4 μmol h^{-1} of hydrogen under UV/vis irradiation. The type of noble metal and its properties are crucial for the photocatalytic performance. Under UV/vis irradiation, only platinum enhances the evolution of hydrogen (2.77 μmol h^{-1}), probably due to the best catalytic (dark) property. In contrast, under vis irradiation, gold enhances the activity of BWO the most, reaching ca. 0.25 μmol h^{-1} of hydrogen generation. Based on the XPS analysis, it has been found that zero-valent metals are the most highly recommended for activity enhancement under vis light, probably due to plasmonic photocatalysis, efficient light harvesting, and the catalytic effect.

Although the obtained data indicated that BWO hierarchical balls are prospective for both hydrogen generation and decomposition of organic compounds, further experiments are necessary to confirm the complete degradation (mineralization) of pollutants, e.g., with the use of a total organic carbon (TOC) analyzer. Moreover, the application of another test compound (colorless) for activity testing to avoid the possibility of photocatalyst sensitization [54,105–107] is under study for the detailed discussion on the reaction mechanisms.

Author Contributions: Conceptualization, Z.W.; methodology, Z.W.; investigation, Z.L. and J.Z.; resources, Z.W.; writing—original draft preparation, Z.W.; writing—review and editing, E.K.; visualization, K.W.; supervision, Y.C., Z.W., and E.K.; funding acquisition, Z.W. All authors have read and agreed to the published version of the manuscript.

Funding: This research was funded by National Natural Science Foundation of China (NSFC) (51802087), the Natural Science Foundation of the Hubei province of China (2019CFB524).

Data Availability Statement: The data presented in this study are available on request from corresponding author (Z.W.).

Conflicts of Interest: The authors declare no conflict of interest.

References

1. Esswein, A.J.; Nocera, D.G. Hydrogen production by molecular photocatalysis. *Chem. Rev.* **2007**, *107*, 4022–4047. [CrossRef]
2. Domen, K.; Naito, S.; Soma, M.; Onishi, T.; Tamaru, K. Photocatalytic decomposition of water vapour on an NiO-$SrTiO_3$ catalyst. *Chem. Commun.* **1980**, *12*, 543–544. [CrossRef]
3. Kudo, A. Recent progress in the development of visible light-driven powdered photocatalysts for water splitting. *Int. J. Hydrog. Energ.* **2007**, *32*, 2673–2678. [CrossRef]
4. Fujishima, A.; Honda, K. Electrochemical photolysis of water at a semiconductor electrode. *Nature* **1972**, *238*, 37–38. [CrossRef]
5. Wei, Z.; Mogan, T.R.; Wang, K.; Janczarek, M.; Kowalska, E. Morphology-governed performance of multi-dimensional photocatalysts for hydrogen generation. *Energies* **2021**, *14*, 7223. [CrossRef]

6. Hoffmann, M.R.; Martin, S.T.; Choi, W.Y.; Bahnemann, D.W. Environmental applications of semiconductor photocatalysis. *Chem. Rev.* **1995**, *95*, 69–96. [CrossRef]
7. Bahnemann, D.W.; Kholuiskaya, S.N.; Dillert, R.; Kulak, A.I.; Kokorin, A.I. Photodestruction of dichloroacetic acid catalyzed by nano-sized TiO_2 particles. *Appl. Catal. B Environ.* **2002**, *36*, 161–169. [CrossRef]
8. Bahnemann, D.; Cunningham, J.; Fox, M.A.; Pelizzetti, E.; Pichat, P.; Serpone, N. Photocatalytic treatment of waters. In *Aquatic and Surface Photochemistry*; CRC Press: Boca Raton, FL, USA, 1994; pp. 261–316.
9. Markowska-Szczupak, A.; Ulfig, K.; Morawski, W.A. The application of titanium dioxide for deactivation of bioparticulates: An overview. *Catal. Today* **2011**, *161*, 249–257. [CrossRef]
10. Mitoraj, D.; Kisch, H. The nature of nitrogen-modified titanium dioxide photocatalysts active in visible light. *Angew. Chem. Int. Ed.* **2008**, *47*, 9975–9978. [CrossRef] [PubMed]
11. Yu, H.; Ming, H.; Zhang, H.; Li, H.; Pan, K.; Liu, Y.; Wang, F.; Gong, J.; Kang, Z. Au/ZnO nanocomposite: Facile fabrication and enhanced photocatalytic activity for degradation of benzene. *Mat. Chem. Phys.* **2012**, *137*, 113–117. [CrossRef]
12. Abe, R.; Shinmei, K.; Koumura, N.; Hara, K.; Ohtani, B. Visible-light-induced water splitting based on two-step photoexcitation between dye-sensitized layered niobate and tungsten oxide photocatalysts in the presence of a triiodide/iodide shuttle redox mediator. *J. Am. Chem. Soc.* **2013**, *135*, 16872–16884. [CrossRef]
13. Malato, S.; Blanco, J.; Caceres, J.; Fernandez-Alba, A.R.; Aguera, A.; Rodriguez, A. Photocatalytic treatment of water-soluble pesticides by photo-Fenton and TiO_2 using solar energy. *Catal. Today* **2002**, *76*, 209–220. [CrossRef]
14. Nakata, K.; Fujishima, A. TiO_2 photocatalysis: Design and applications. *J. Photoch. Photobio. C* **2012**, *13*, 169–189. [CrossRef]
15. Ochiai, T.; Fujishima, A. Photoelectrochemical properties of TiO_2 photocatalyst and its applications for environmental purification. *J. Photoch. Photobio. C* **2012**, *13*, 247–262. [CrossRef]
16. Kowalska, E.; Rau, S. Photoreactors for wastewater treatment: A review. *Recent Pat. Engin.* **2010**, *4*, 242–266. [CrossRef]
17. Bielan, Z.; Dudziak, S.; Kubiak, A.; Kowalska, E. Application of spinel and hexagonal ferrites in heterogeneous photocatalysis. *Appl. Sci.* **2021**, *11*, 10160. [CrossRef]
18. Grzechulska, J.; Morawski, A.W. Photocatalytic labyrinth flow reactor with immobilized P25 TiO_2 bed for removal of phenol from water. *Appl. Catal. B Environ.* **2003**, *46*, 415–419. [CrossRef]
19. Zabek, P.; Eberl, J.; Kisch, H. On the origin of visible light activity in carbon-modified titania. *Photochem. Photobiol. Sci.* **2009**, *8*, 264–269. [CrossRef] [PubMed]
20. Dozzi, M.V.; Prati, L.; Canton, P.; Selli, E. Effects of gold nanoparticles deposition on the photocatalytic activity of titanium dioxide under visible light. *Phys. Chem. Chem. Phys.* **2009**, *11*, 7171–7180. [CrossRef]
21. Janus, M.; Tryba, B.; Inagaki, M.; Morawski, A.W. New preparation of a carbon-TiO_2 photocatalyst by carbonization of n-hexane deposited on TiO_2. *Appl. Catal. B Environ.* **2004**, *52*, 61–67. [CrossRef]
22. Zaleska, A. Doped-TiO_2: A review. *Rec. Patent. Eng.* **2008**, *2*, 157–164. [CrossRef]
23. Asahi, R.; Morikawa, T.; Ohwaki, T.; Aoki, K.; Taga, Y. Visible-light photocatalysis in nitrogen-doped titanium oxides. *Science* **2001**, *293*, 269–271. [CrossRef]
24. Ohno, T.; Mitsui, T.; Matsumura, M. Photocatalytic activity of S-doped TiO_2 photocatalyst under visible light. *Chem. Lett.* **2003**, *32*, 364–365. [CrossRef]
25. Hsu, M.-H.; Chang, C.-J.; Weng, H.-T. Efficient H_2 production using Ag_2S-coupled ZnO@ZnS core–shell nanorods decorated metal wire mesh as an immobilized hierarchical photocatalyst. *ACS Sustain. Chem. Eng.* **2016**, *4*, 1381–1391. [CrossRef]
26. Endo-Kimura, M.; Janczarek, M.; Bielan, Z.; Zhang, D.; Wang, K.; Markowska-Szczupak, A.; Kowalska, E. Photocatalytic and antimicrobial properties of Ag_2O/TiO_2 heterojunction. *ChemEngineering* **2019**, *3*, 3. [CrossRef]
27. Janczarek, M.; Endo, M.; Zhang, D.; Wang, K.; Kowalska, E. Enhanced photocatalytic and antimicrobial performance of cuprous oxide/titania: The effect of titania matrix. *Materials* **2018**, *11*, 2069. [CrossRef] [PubMed]
28. Zhang, P.; Zhang, L.; Dong, E.; Zhang, X.; Zhang, W.; Wang, Q.; Xu, S.; Li, H. Synthesis of $CaIn_2S_4/TiO_2$ heterostructures for enhanced UV–visible light photocatalytic activity. *J. Alloys Compd.* **2021**, *885*, 161027. [CrossRef]
29. Yashima, M.; Maeda, K.; Teramura, K.; Takata, T.; Domen, K. Crystal structure and optical properties of $(Ga_{1-x}Zn_x)(N_{1-x}O_x)$ oxynitride photocatalyst (x = 0.13). *Chem. Phys. Lett.* **2005**, *416*, 225–228. [CrossRef]
30. Maeda, K.; Wang, X.; Nishihara, Y.; Lu, D.; Antonietti, M.; Domen, K. Photocatalytic activities of graphitic carbon nitride powder for water reduction and oxidation under visible light. *J. Phys. Chem. C* **2009**, *113*, 4940–4947. [CrossRef]
31. Sato, J.; Saito, N.; Yamada, Y.; Maeda, K.; Takata, T.; Kondo, J.N.; Hara, M.; Kobayashi, H.; Domen, K.; Inoue, Y. RuO_2-loaded beta-Ge_3N_4 as a non-oxide photocatalyst for overall water splitting. *J. Am. Chem. Soc.* **2005**, *127*, 4150–4151. [CrossRef] [PubMed]
32. Fakhri, H.; Farzadkia, M.; Boukherroub, R.; Srivastava, V.; Sillanpaa, M. Design and preparation of core-shell structured magnetic graphene oxide@MIL-101(Fe): Photocatalysis under shell to remove diazinon and atrazine pesticides. *Sol. Energy* **2020**, *208*, 990–1000. [CrossRef]
33. Liang, H.; Bai, J.; Xu, T.; Li, C. In-situ synthesized and photocatalytic performance evaluation of MoS_2-C-g-C_3N_4 heterostructure photocatalyts. *Adv. Powder. Technol.* **2021**, *32*, 4805–4813. [CrossRef]
34. Enesca, A.; Isac, L.; Duta, A. Charge carriers injection in tandem semiconductors for dyes mineralization. *Appl. Catal. B Environ.* **2015**, *162*, 352–363. [CrossRef]
35. Jin, X.; Ye, L.; Xie, H.; Chen, G. Bismuth-rich bismuth oxyhalides for environmental and energy photocatalysis. *Coord. Chem. Rev.* **2017**, *349*, 84–101. [CrossRef]

36. Zhang, L.W.; Baumanis, C.; Robben, L.; Kandiel, T.; Bahnemann, D. Bi_2WO_6 inverse opals: Facile fabrication and efficient visible-light-driven photocatalytic and photoelectrochemical water-splitting activity. *Small* **2011**, *7*, 2714–2720. [CrossRef]
37. Zhang, L.; Wang, W.; Zhou, L.; Xu, H. Bi_2WO_6 nano—and microstructures: Shape control and associated visible-light-driven photocatalytic activities. *Small* **2007**, *3*, 1618–1625. [CrossRef]
38. Zhang, C.; Zhu, Y. Synthesis of square Bi_2WO_6 nanoplates as high-activity visible-light-driven photocatalysts. *Chem. Mater.* **2005**, *17*, 3537–3545. [CrossRef]
39. Fu, H.; Pan, C.; Yao, W.; Zhu, Y. Visible-light-induced degradation of rhodamine B by nanosized Bi_2WO_6. *J. Phys. Chem. B* **2005**, *109*, 22432–22439. [CrossRef] [PubMed]
40. Yang, Z.; Huang, L.; Xie, Y.; Lin, Z.; Fan, Y.; Liu, D.; Chen, L.; Zhang, Z.; Wang, X. Controllable synthesis of Bi_2WO_6 nanoplate self-assembled hierarchical erythrocyte microspheres via a one-pot hydrothermal reaction with enhanced visible light photocatalytic activity. *Appl. Surf. Sci.* **2017**, *403*, 326–334. [CrossRef]
41. Li, Y.; Liu, J.; Huang, X. Synthesis and visible-light photocatalytic property of Bi_2WO_6 hierarchical octahedron-like structures. *Nanoscale Res. Lett.* **2008**, *3*, 365–371. [CrossRef]
42. Deng, X.-X.; Tian, S.; Chai, Z.-M.; Bai, Z.-J.; Tan, Y.-X.; Chen, L.; Guo, J.-K.; Shen, S.; Cai, M.-Q.; Au, C.-T.; et al. Boosted activity for toluene selective photooxidation over Fe-doped Bi_2WO_6. *Ind. Eng. Chem. Res.* **2020**, *59*, 13528–13538. [CrossRef]
43. Zhu, D.; Zhou, Q. Novel Bi_2WO_6 modified by N-doped graphitic carbon nitride photocatalyst for efficient photocatalytic degradation of phenol under visible light. *Appl. Cata. B Environ.* **2020**, *268*, 118426. [CrossRef]
44. Yuan, C.; Gao, H.; Xu, Q.; Song, X.; Zhai, C.; Zhu, M. Pt decorated 2D/3D heterostructure of Bi_2WO_6 nanosheet/Cu_2S snowflake for improving electrocatalytic methanol oxidation with visible-light assistance. *Appl. Surf. Sci.* **2020**, *521*, 146431. [CrossRef]
45. Wang, R.; Li, B.; Xiao, Y.; Tao, X.; Su, X.; Dong, X. Optimizing Pd and Au-Pd decorated Bi_2WO_6 ultrathin nanosheets for photocatalytic selective oxidation of aromatic alcohols. *J. Catal.* **2018**, *364*, 154–165. [CrossRef]
46. Yu, Y.-N.; Lu, S.-Y.; Bao, S.-J. Photocatalytic activity of Pt-modified Bi_2WO_6 nanoporous wall under sunlight. *J. Nanopart. Res.* **2015**, *17*, 323. [CrossRef]
47. Wu, Q.-S.; Cui, Y.; Yang, L.; Zhang, G.-Y.; Gao, D.Z. Facile in-situ photocatalysis of Ag/Bi_2WO_6 heterostructure with obviously enhanced performance. *Sep. Purif. Technol.* **2015**, *142*, 168–175. [CrossRef]
48. Ma, T.; Liu, C.; Li, Z.; Zheng, R.; Chen, M.; Dai, S.; Zhao, T. Mechanochemically constructed Bi_2WO_6/Zn-Al layered double hydroxide heterojunction with prominent visible light-driven photocatalytic efficiency. *Appl. Clay Sci.* **2021**, *215*, 106328. [CrossRef]
49. Li, B.; Lai, C.; Zeng, G.; Qin, L.; Yi, H.; Huang, D.; Zhou, C.; Liu, X.; Cheng, M.; Xu, P.; et al. Facile hydrothermal synthesis of Z-Scheme $Bi_2Fe_4O_9$/Bi_2WO_6 heterojunction photocatalyst with enhanced visible light photocatalytic activity. *ACS Appl. Mater. Interf.* **2018**, *10*, 18824–18836. [CrossRef]
50. Wang, F.; Li, W.; Gu, S.; Li, H.; Wu, X.; Ren, C.; Liu, X. Facile fabrication of direct Z-scheme MoS_2/Bi_2WO_6 heterojunction photocatalyst with superior photocatalytic performance under visible light irradiation. *J. Photochem. Photobiol. A Chem.* **2017**, *335*, 140–148. [CrossRef]
51. Kraeutler, B.; Bard, A.J. Heterogeneous photocatalytic preparation of supported catalysts. Photodeposition of platinum on TiO_2 powder and other substrates. *J. Am. Chem. Soc.* **1978**, *100*, 4317–4318. [CrossRef]
52. Herrmann, J.M.; Disdier, J.; Pichat, P.; Fernandez, A.; Gonzalez-Elipe, A.; Munuera, G.; Leclercq, C. Titania-supported bimetallic catalyst synthesis by photocatalytic codeposition at ambient temperature: Preparation and characterization of platinum-rhodium, silver-rhodium, and platinum-palladium couples. *J. Catal.* **1991**, *132*, 490–497. [CrossRef]
53. Ohtani, B.; Kakimoto, M.; Nishimoto, S.; Kagiya, T. Photocatalytic reaction of neat alcohols by metal-loaded titanium(IV) oxide particles. *J. Phys. Chem. A Chem.* **1993**, *70*, 265–272. [CrossRef]
54. Kowalska, E.; Remita, H.; Colbeau-Justin, C.; Hupka, J.; Belloni, J. Modification of titanium dioxide with platinum ions and clusters: Application in photocatalysis. *J. Phys. Chem. C* **2008**, *112*, 1124–1131. [CrossRef]
55. Phuruangrat, A.; Putdum, S.; Dumrongrojthanath, P.; Ekthammathat, N.; Thongtem, S.; Thongtem, T. Enhanced properties for visible-light-driven photocatalysis of Ag nanoparticle modified Bi_2MoO_6 nanoplates. *Mater. Sci. Semicond. Process.* **2015**, *34*, 175–181. [CrossRef]
56. Gao, Y.; Wang, L.; Li, Z.; Li, C.; Cao, X.; Zhou, A.; Hu, Q. Microwave-assisted synthesis of flower-like Ag–BiOCl nanocomposite with enhanced visible-light photocatalytic activity. *Mater. Lett.* **2014**, *136*, 295–297. [CrossRef]
57. Chang, Y.; Liu, Z.; Shen, X.; Zhu, B.; Macharia, D.K.; Chen, Z.; Zhang, L. Synthesis of Au nanoparticle-decorated carbon nitride nanorods with plasmon-enhanced photoabsorption and photocatalytic activity for removing various pollutants from water. *J. Hazard. Mater.* **2018**, *344*, 1188–1197. [CrossRef]
58. Dong, Q.; Chen, Y.; Wang, L.; Ai, S.; Ding, H. Cu-modified alkalinized g-C_3N_4 as photocatalytically assisted heterogeneous Fenton-like catalyst. *Appl. Surf. Sci.* **2017**, *426*, 1133–1140. [CrossRef]
59. Meng, X.; Li, Z.; Chen, J.; Xie, H.; Zhang, Z. Enhanced visible light-induced photocatalytic activity of surface-modified BiOBr with Pd nanoparticles. *Appl. Surf. Sci.* **2018**, *433*, 76–87. [CrossRef]
60. Tian, Y.; Tatsuma, T. Mechanisms and applications of plasmon-induced charge separation at TiO_2 films loaded with gold nanoparticles. *J. Am. Chem. Soc.* **2005**, *127*, 7632–7637. [CrossRef] [PubMed]
61. Verbruggen, S.W. TiO_2 photocatalysis for the degradation of pollutants in gas phase: From morphological design to plasmonic enhancement. *J. Photoch. Photobio. C* **2015**, *24*, 64–82. [CrossRef]

62. Kowalska, E.; Abe, R.; Ohtani, B. Visible light-induced photocatalytic reaction of gold-modified titanium(IV) oxide particles: Action spectrum analysis. *Chem. Commun.* **2009**, *2*, 241–243. [CrossRef] [PubMed]
63. Kadam, A.; Dhabbe, R.; Gophane, A.; Sathe, T.; Garadkar, K. Template free synthesis of ZnO/Ag_2O nanocomposites as a highly efficient visible active photocatalyst for detoxification of methyl orange. *J. Photochem. Photobiol. B* **2016**, *154*, 24–33. [CrossRef]
64. Morgan, W.E.; Stec, W.J.; Van Wazer, J.R. Inner-orbital binding-energy shifts of antimony and bismuth compounds. *Inorg. Chem.* **1973**, *12*, 953–955. [CrossRef]
65. Fu, Y.; Chang, C.; Chen, P.; Chu, X.; Zhu, L. Enhanced photocatalytic performance of boron doped Bi_2WO_6 nanosheets under simulated solar light irradiation. *J. Hazard. Mater.* **2013**, *254–255*, 185–192. [CrossRef] [PubMed]
66. Zhang, F.-J.; Zhu, S.-F.; Xie, F.-Z.; Zhang, J.; Meng, Z.-D. Plate-on-plate structured Bi_2MoO_6/Bi_2WO_6 heterojunction with high-efficiently gradient charge transfer for decolorization of MB. *Sep. Purif. Technol.* **2013**, *113*, 1–8. [CrossRef]
67. Xu, X.; Meng, L.; Li, Y.; Sun, C.; Yang, S.; He, H. Bi_2S_3 nanoribbons-hybridized {001} facets exposed Bi_2WO_6 ultrathin nanosheets with enhanced visible light photocatalytic activity. *Appl. Surf. Sci.* **2019**, *479*, 410–422. [CrossRef]
68. Fleisch, T.H.; Zajac, G.W.; Schreiner, J.O.; Mains, G.J. An XPS study of the UV photoreduction of transition and noble metal oxides. *Appl. Surf. Sci.* **1986**, *26*, 488–497. [CrossRef]
69. Endo-Kimura, M.; Karabiyik, B.; Wang, K.; Wei, Z.; Ohtani, B.; Markowska-Szczupak, A.; Kowalska, E. Vis-responsive copper-modified titania for decomposition of organic compounds and microorganisms. *Catalysts* **2020**, *10*, 1194. [CrossRef]
70. Wei, Z.; Endo, M.; Wang, K.; Charbit, E.; Markowska-Szczupak, A.; Ohtani, B.; Kowalska, E. Noble metal-modified octahedral anatase titania particles with enhanced activity for decomposition of chemical and microbiological pollutants. *Chem. Eng. J.* **2017**, *318*, 121–134. [CrossRef] [PubMed]
71. Janczarek, M.; Wei, Z.; Endo, M.; Ohtani, B.; Kowalska, E. Silver- and copper-modified decahedral anatase tiania particles as visible light-responsive plasmonic photocatalyst. *J. Photon. Energy* **2017**, *7*, 1–16.
72. Zhang, J.; Chen, T.; Lu, H.; Yang, Z.; Yin, F.; Gao, J.; Liu, Q.; Tu, Y. Hierarchical Bi_2WO_6 architectures decorated with Pd nanoparticles for enhanced visible-light-driven photocatalytic activities. *Appl. Surf. Sci.* **2017**, *404*, 282–290. [CrossRef]
73. Wei, Z.; Janczarek, M.; Endo, M.; Colbeau-Justin, C.; Ohtani, B.; Kowalska, E. Silver-modified octahedral anatase particles as plasmonic photocatalyst. *Catal. Today* **2018**, *310*, 19–25. [CrossRef] [PubMed]
74. Wei, Z.; Janczarek, M.; Endo, M.; Wang, K.L.; Balcytis, A.; Nitta, A.; Mendez-Medrano, M.G.; Colbeau-Justin, C.; Juodkazis, S.; Ohtani, B.; et al. Noble metal-modified faceted anatase titania photocatalysts: Octahedron versus decahedron. *Appl. Catal. B Environ.* **2018**, *237*, 574–587. [CrossRef] [PubMed]
75. Zheng, S.; Wei, Z.; Yoshiiri, K.; Braumuller, M.; Ohtani, B.; Rau, S.; Kowalska, E. Titania modification with ruthenium(II) complex and gold nanoparticles for photocatalytic degradation of organic compounds. *Photochem. Photobiol. Sci.* **2016**, *15*, 69–79. [CrossRef] [PubMed]
76. Mukherji, S.; Bharti, S.; Shukla, G.; Mukherji, S. Synthesis and characterization of size- and shape-controlled silver nanoparticles. *Phys. Sci. Rev.* **2018**, *4*, 20170082.
77. Xia, Y.N.; Halas, N.J. Shape-controlled synthesis and surface plasmonic properties of metallic nanostructures. *Mrs Bull.* **2005**, *30*, 338–344. [CrossRef]
78. Sugawa, K.; Tahara, H.; Yamashita, A.; Otsuki, J.; Sagara, T.; Harumoto, T.; Yanagida, S. Refractive index susceptibility of the plasmonic palladium nanoparticle: Potential as the third plasmonic sensing material. *ACS Nano* **2015**, *9*, 1895–1904. [CrossRef] [PubMed]
79. Zielinska-Jurek, A.; Wei, Z.; Wysocka, I.; Szweda, P.; Kowalska, E. The effect of nanoparticles size on photocatalytic and antimicrobial properties of Ag-Pt/TiO_2 photocatalysts. *Appl. Surf. Sci.* **2015**, *353*, 317–325. [CrossRef]
80. Kowalska, E.; Wei, Z.; Karabiyik, B.; Herissan, A.; Janczarek, M.; Endo, M.; Markowska-Szczupak, A.; Remita, H.; Ohtani, B. Silver-modified titania with enhanced photocatalytic and antimicrobial properties under UV and visible light irradiation. *Catal. Today* **2015**, *252*, 136–142. [CrossRef]
81. Kowalska, E.; Mahaney, O.O.P.; Abe, R.; Ohtani, B. Visible-light-induced photocatalysis through surface plasmon excitation of gold on titania surfaces. *Phys. Chem. Chem. Phys.* **2010**, *12*, 2344–2355. [CrossRef]
82. Muniz-Miranda, M.; Gellini, C.; Simonelli, A.; Tiberi, M.; Giammanco, F.; Giorgetti, E. Characterization of copper nanoparticles obtained by laser ablation in liquids. *Appl. Phys. A Mater.* **2013**, *110*, 829–833. [CrossRef]
83. Mendez-Medrano, M.G.; Kowalska, E.; Ohtani, B.; Uribe, D.B.; Colbeau-Justin, C.; Rau, S.; Rodriguez-Lopez, J.L.; Remita, H. Heterojunction of CuO nanoclusters with TiO_2 for photo-oxidation of organic compounds and for hydrogen production. *J. Chem. Phys.* **2020**, *153*, 034705. [CrossRef]
84. Mendez-Medrano, M.G.; Kowalska, E.; Lehoux, A.; Herissan, A.; Ohtani, B.; Bahena, D.; Briois, V.; Colbeau-Justin, C.; Rodriguez-Lopez, J.; Remita, H. Surface modification of TiO_2 with Ag nanoparticles and CuO nanoclusters for applications in photocatalysis. *J. Phys. Chem. C* **2016**, *120*, 5143–5154. [CrossRef]
85. Luna, A.L.; Valenzuela, M.A.; Colbeau-Justin, C.; Vazquez, P.; Rodriguez, J.L.; Avendano, J.R.; Alfaro, S.; Tirado, S.; Garduno, A.; De la Rosa, J.M. Photocatalytic degradation of gallic acid over CuO–TiO_2 composites under UV/Vis LEDs irradiation. *Appl. Catal. A Gen.* **2016**, *521*, 140–148. [CrossRef]
86. Ito, T.; Yamaguchi, H.; Masumi, T.; Adachi, S. Optical properties of CuO studied by spectroscopic ellipsometry. *J. Phys. Soc. Jpn.* **1998**, *67*, 3304–3309. [CrossRef]

87. Abe, R. Recent progress on photocatalytic and photoelectrochemical water splitting under visible light irradiation. *J. Photoch. Photobio. C* **2010**, *11*, 179–209. [CrossRef]
88. Abe, R.; Takami, H.; Murakami, N.; Ohtani, B. Pristine simple oxides as visible light driven photocatalysts: Highly efficient decomposition of organic compounds over platinum-loaded tungsten oxide. *J. Am. Chem. Soc.* **2008**, *130*, 7780–7781. [CrossRef] [PubMed]
89. Hori, H.; Takashima, M.; Takase, M.; Ohtani, B. Kinetic analysis supporting multielectron reduction of oxygen in bismuth tungstate-photocatalyzed oxidation of organic compounds. *Catal. Today* **2018**, *313*, 218–223. [CrossRef]
90. Wang, K.L.; Wei, Z.S.; Ohtani, B.; Kowalska, E. Interparticle electron transfer in methanol dehydrogenation on platinum-loaded titania particles prepared from P25. *Catal. Today* **2018**, *303*, 327–333. [CrossRef]
91. Wei, Z.; Kowalska, E.; Wang, K.; Colbeau-Justin, C.; Ohtani, B. Enhanced photocatalytic activity of octahedral anatase particles prepared by hydrothermal reaction. *Catal. Today* **2017**, *280*, 29–36. [CrossRef]
92. Wei, Z.; Rosa, L.; Wang, K.; Endo, M.; Juodkazi, S.; Ohtani, B.; Kowalska, E. Size-controlled gold nanoparticles on octahedral anatase particles as efficient plasmonic photocatalyst. *Appl. Catal. B Environ.* **2017**, *206*, 393–405. [CrossRef] [PubMed]
93. Kowalska, E.; Yoshiiri, K.; Wei, Z.; Zheng, S.; Kastl, E.; Remita, H.; Ohtani, B.; Rau, S. Hybrid photocatalysts composed of titania modified with plasmonic nanoparticles and ruthenium complexes for decomposition of organic compounds. *Appl. Catal. B Environ.* **2015**, *178*, 133–143. [CrossRef]
94. Kowalska, E.; Janczarek, M.; Rosa, L.; Juodkazi, S.; Ohtani, B. Mono- and bi-metallic plasmonic photocatalysts for degradation of organic compounds under UV and visible light irradiation. *Catal. Today* **2014**, *230*, 131–137. [CrossRef]
95. Luna, A.L.; Dragoe, D.; Wang, K.L.; Beaunier, P.; Kowalska, E.; Ohtani, B.; Uribe, D.B.; Valenzuela, M.A.; Remita, H.; Colbeau-Justin, C. Photocatalytic hydrogen evolution using Ni-Pd/TiO_2: Correlation of light absorption, charge-carrier dynamics, and quantum efficiency. *J. Phys. Chem. C* **2017**, *121*, 14302–14311. [CrossRef]
96. Luna, A.L.; Novoseltceva, E.; Louran, E.; Beaunier, P.; Kowalska, E.; Ohtani, B.; Valenzuela, M.A.; Remita, H.; Colbeau-Justin, C. Synergetic effect of Ni and Au nanoparticles synthesized on titania particles for efficient photocatalytic hydrogen production. *Appl. Catal. B Environ.* **2016**, *191*, 18–28. [CrossRef]
97. Hori, H.; Takashima, M.; Takase, M.; Ohtani, B. Pristine bismuth-tungstate photocatalyst particles driving organics decomposition through multielectron reduction of oxygen. *Chem. Lett.* **2017**, *46*, 1376–1378. [CrossRef]
98. Wu, S.; Sun, J.; Li, Q.; Hood, Z.D.; Yang, S.; Su, T.; Peng, R.; Wu, Z.; Sun, W.; Kent, P.R.C.; et al. Effects of surface terminations of 2D Bi_2WO_6 on photocatalytic hydrogen evolution from water splitting. *ACS Appl. Mater. Interfaces* **2020**, *12*, 20067–20074. [CrossRef] [PubMed]
99. Zeng, M.; Li, Y. Recent advances in heterogeneous electrocatalysts for the hydrogen evolution reaction. *J. Mater. Chem. A* **2015**, *3*, 14942–14962. [CrossRef]
100. Wei, Z.; Janczarek, M.; Wang, K.; Zheng, S.; Kowalska, E. Morphology-governed performance of plasmonic photocatalysts. *Catalysts* **2020**, *10*, 1070. [CrossRef]
101. Furube, A.; Du, L.; Hara, K.; Katoh, R.; Tachiya, M. Ulltrafast plasmon-induced electron transfer from gold nanodots into TiO_2 nanoparticles. *J. Am. Chem. Soc.* **2007**, *129*, 14852–14853. [CrossRef] [PubMed]
102. Cushing, S.K.; Wu, N.Q. Progress and perspectives of plasmon-enhanced solar energy conversion. *J. Phys. Chem. Lett.* **2016**, *7*, 666–675. [CrossRef] [PubMed]
103. Wang, K.; Bielan, Z.; Endo-Kimura, M.; Janczarek, M.; Zhang, D.; Kowalski, D.; Zielińska-Jurek, A.; Markowska-Szczupak, A.; Ohtani, B.; Kowalska, E. On the mechanism of photocatalytic reactions on Cu_xO@TiO_2 core–shell photocatalysts. *J. Mat. Chem. A* **2021**, *9*, 10135–10145. [CrossRef]
104. Janczarek, M.; Wang, K.L.; Kowalska, E. Synergistic effect of Cu_2O and urea as modifiers of TiO_2 for enhanced visible light activity. *Catalysts* **2018**, *8*, 240. [CrossRef]
105. Yan, X.; Ohno, T.; Nishijima, K.; Abe, R.; Ohtani, B. Is Methylene blue an appropriate substrate for a photocatalytic activity test? A study with visible-light responsive titania. *Chem. Phys. Lett.* **2006**, *429*, 606–610. [CrossRef]
106. Rochkind, M.; Pasternak, S.; Paz, Y. Using dyes for evaluating photocatalytic properties: A critical review. *Molecules* **2015**, *20*, 88–110. [CrossRef]
107. Barbero, N.; Vione, D. Why dyes should not be used to test the photocatalytic activity of semiconductor oxides. *Environ. Sci. Technol.* **2016**, *50*, 2130–2131. [CrossRef] [PubMed]